

Title: **CT and MR imaging of Bone Tumors**

Authors: **Ladd LM and Roth TD.**

Lauren M. Ladd, MD\*  
Assistant Professor of Radiology  
Department of Radiology and Imaging Sciences  
Indiana University Health / Indiana University School of Medicine  
Indianapolis, IN

Trenton D. Roth  
Assistant Professor of Radiology  
Department of Radiology and Imaging Sciences  
Indiana University Health / Indiana University School of Medicine  
Indianapolis, IN

From: Department of Radiology and Imaging Sciences  
Indiana University Health / Indiana University School of Medicine  
Indianapolis, IN

\*Corresponding author: Lauren Ladd, MD

LMLadd@iupui.edu  
317-962-8767 (work)  
1701 N. Senate Blvd.  
Radiology Dept, MH1238A  
Indianapolis, IN 46202

## **ABSTRACT**

Imaging is the key to diagnosing and guiding management of bone tumors. Although radiographs are the gold standard for initial imaging evaluation and may make the diagnosis, computed tomography (CT) and magnetic resonance (MR) imaging are important adjunct tools for further characterization as a benign or aggressive lesion, accurately determining matrix composition, assessing lesion extent as well as secondary involvement of nearby structures if malignant, and staging tumors when applicable. In this article, we will highlight important features of CT and MR imaging for bone tumor

---

This is the author's manuscript of the article published in final edited form as:

Ladd, L. M., & Roth, T. D. (2017). Computed Tomography and Magnetic Resonance Imaging of Bone Tumors. *Seminars in Roentgenology*. <https://doi.org/10.1053/j.ro.2017.04.006>

evaluation and review the cross-sectional imaging features of a broad spectrum of benign and malignant bone tumors.

## INTRODUCTION

Malignant primary bone tumors make up only 0.2% of all malignancies in adults<sup>1,2</sup> and 5% in children from ages 5-15 years old.<sup>1,3</sup> Benign bone tumors are more common, but the true prevalence is unknown because they are often asymptomatic and go undiscovered. The clinical presentation of bone tumors can be challenging. The nonspecific gradual onset of pain and swelling in most malignant tumors and asymptomatic nature of many benign tumors<sup>1,4</sup> reinforces the importance of the radiologist's role in detecting, working up, and staging bone lesions. It is important for radiologists to recognize imaging features that can distinguish non-aggressive incidental tumors from those that are aggressive or potentially malignant. In some cases, a specific diagnosis may be rendered based on patient age, lesion location, and recognition of characteristic imaging features. In other cases, a short list of the most likely differential diagnoses can be provided to help guide further workup and management.

Furthermore, imaging plays a central role in the staging of malignant bone tumors. For over 30 years, a bone tumor-specific system by Enneking, et al, has been used<sup>5</sup>. While this is still used by some orthopedists and extensively used in the radiology literature, the recent focus on multidisciplinary team-based care has resulted in a shift to use the American Joint Commission on Cancer (AJCC) system. Both classifications are discussed in a review by Balach and colleagues.<sup>4</sup>

## IMAGING

Given the importance of imaging in bone tumor evaluation, the radiologist should be involved early on to help guide the most appropriate imaging technique(s). Key imaging information for the orthopedist includes the following: the character of the lesion (benign or aggressive), size and location of the lesion (including in relation to clinical landmarks), involved compartments, presence of skip metastases, relationship to neurovascular structures, intra-articular extension, and potential for imaging-guided needle biopsy.<sup>6</sup>

### *Radiography*

Radiographs are the gold standard and first line imaging for tumor evaluation.<sup>7</sup> The radiographic appearance indicates the lesion aggressiveness and establishes the differential and/or diagnosis.<sup>8</sup> Key radiographic features include the location, margins, matrix, periosteal reaction, and general aggressiveness of the lesion.<sup>9,10</sup> From the patient history, age, lesion location, and radiographic appearance, 80% of bone lesions may be correctly identified.<sup>6</sup> In appropriate cases, cross sectional imaging further characterizes the lesion, and in cases of aggressive or malignant disease is critical to determine extent of disease and stage the tumor. This information has revolutionized surgical treatment, enabling limb salvage, which was nonexistent 30 years ago.<sup>11</sup>

### *Computed Tomography*

Depending on the radiographic appearance and differential diagnosis, CT or MR imaging are the next best imaging techniques according to the ACR Appropriateness Criteria.<sup>7</sup>

High spatial resolution CT provides exquisite detail of cortical and trabecular bone, making it an important tool in a variety of cases and specific tumors. For example, CT is the exam of choice for specific diagnoses, such as osteoid osteoma.<sup>1</sup> CT is better than MR imaging at evaluating cortical involvement, destruction, or breakthrough; matrix mineralization; and periosteal reaction.<sup>9-12</sup> Structural integrity or risk of impending pathologic fractures may also be inferred by evaluation of cortical involvement,<sup>4</sup> and 3D reconstructions can be helpful evaluating surface lesions.<sup>12</sup> Further, lesions in complex or flat bones, such as the pelvis, spine, scapula, and ribs, are often poorly visualized on radiographs, making CT the imaging technique of choice for such bones.<sup>4,9,11,12</sup>

CT imaging of bone lesions is performed with thin collimation and high detail technique. Thin section axial, coronal, and sagittal multiplanar reformations are created, typically using a bone filter, though additional axial reformatted images with a soft tissue filter may also be created to better assess soft tissue components or intramuscular extension. Intravenous contrast media may be useful in assessing non-osseous soft tissue components of the tumor.

### *Magnetic Resonance Imaging*

The superior soft tissue contrast of MR imaging makes it often the most appropriate study to evaluate a bone tumor after radiography.<sup>7</sup> Details of the intramedullary and extraosseous extent of a tumor, presence of an associated soft tissue mass, and involvement of adjacent structures, including neurovascular bundles, intra-articular space, and muscle or adjacent fat planes, are best seen with MR.<sup>1,4,9,10,12,13</sup> According to

multiple studies, MR imaging was superior to CT in assessing bone marrow involvement (33-38%) and soft tissue tumor extent (38-54%), as well as neurovascular (69%) and joint involvement (100%).<sup>10,14</sup> Intratumoral necrosis versus viable tissue may also be delineated on MR imaging, which aids in biopsy planning. For these many reasons, MR imaging plays a crucial role in staging musculoskeletal lesions and planning for appropriate limb salvage when applicable.<sup>11</sup>

The imaging characteristics of tumors will be discussed individually below. However, neurovascular bundle involvement is characterized by soft tissue surrounding at least 180 degrees of the bundle (best seen on axial images), and joint involvement is defined by disruption of the joint capsule or articular subchondral bone plate/cartilage on T1 images.<sup>10</sup>

The mainstay of MR imaging of tumors is multiple orthogonal spin echo T1- and T2-weighted sequences. The soft tissue contrast and ability to differentiate tissue compositions is due to the different and adaptable imaging parameters and sequences. Evaluation of tumors should include at least one large field-of-view (FOV) sequence to survey the entire bone for tumor extent and skip metastases. A large FOV sacrifices spatial resolution, however, so a small FOV and surface coil should be used for the remainder of the exam to ensure the best resolution possible.<sup>4,6</sup> At our institution, tumor MR imaging protocols include T1, T2 fat-suppressed (T2FS) or short tau inversion recovery (STIR), and post-contrast T1 fat-suppressed (T1FS+C) sequences in axial, coronal, and sagittal planes. The added time for all three planes (rather than just two

planes) may be warranted due to the uncertainty of the best imaging orientation with respect to the lesion.<sup>15</sup> Chemical shift imaging with in- and out-of-phase gradient echo sequences may be added to an examination for problem solving, where lack of out-of-phase signal dropout indicates marrow fat replacement.<sup>16,17</sup>

### *Advanced Imaging*

Advanced imaging is beyond the scope of this article but includes advanced MR techniques and positron emission tomography (PET)-CT. MR dynamic contrast enhancement has demonstrated promise delineating between viable tumor (rapid enhancement) versus posttreatment change (slow enhancement).<sup>1,18</sup> MR spectroscopy and diffusion imaging are also being studied for their utility in identification of benign versus malignant bone lesions, as well as differentiation between tumor and peritumoral edema, both after chemotherapy and surgery.<sup>4,15,16</sup> Lastly, PET-CT, the gold standard in metabolic imaging, has been extensively studied as a problem-solving tool in sarcoma imaging and is most often used to help determine the most active regions for biopsy planning, to detect metastatic disease, and to evaluate posttreatment response.<sup>4,15,16</sup> Unfortunately, there is significant overlap in SUV measurements for benign and malignant bone lesions, thus there is limited utility in determining the underlying etiology of a bone lesion with PET imaging.

## **BONE TUMORS**

There are many ways to group and differentiate tumors, including by location,<sup>19</sup> age,<sup>9</sup> cell type,<sup>1</sup> and imaging appearance. The World Health Organization classifies bone tumors by

origin of cell type. We will modify this approach and use the tissue composition or matrix, a consequence of the cell origin, to work through a differential list of select bone tumors, highlighting the appearances on CT and MR imaging.

### *Osteoid tumors*

Osteoid tumors range from benign osteoid osteomas and osteblastomas to a spectrum of various osteosarcomas. These bone-forming lesions have distinct osteoid composition, often with characteristic mineralization pattern, to help differentiate from tumor of other compositions and histologic origins.

Osteoid osteomas comprise 10% of all benign bone tumors, and are usually found in young patients (5-30 years).<sup>20</sup> They frequently occur in long bones (>50% in tibia and femur), spine (90% in posterior elements), and feet with hallmark symptoms of dull aching pain that is worse at night and relieved by salicylates.<sup>20-22</sup> Spine lesions may present with new-onset painful scoliosis.<sup>20-22</sup>

Histologically, osteoid osteomas are a small (1mm - 2cm) nidus of richly innervated osteoid and woven bone on a background of vascularized fibrous connective tissue.<sup>20,21</sup>

The nidus is radiolucent with variable mineralization, which may be evident radiographically but is better seen with CT, the imaging method of choice because of the spatial resolution. Intracortical osteoid osteomas (70%) cause reactive cortical thickening and benign periosteal new bone formation around the radiolucent nidus, which are also best assessed on CT (Fig. 1).<sup>20,22</sup> When located in medullary, subperiosteal, or intra-

articular locations, sclerosis and periostitis are less common, making nidus identification by CT the key to the appropriate diagnosis.<sup>20</sup> Subperiosteal osteoid osteomas, classically at the femoral neck, may demonstrate the nidus with shallow scalloping of the underlying cortex. Intra-articular lesions are also difficult to diagnose, sometimes only demonstrating secondary signs of a reactive joint effusion, synovitis, or periarticular osteopenia.<sup>21</sup>

MR imaging of osteoid osteomas is variable and may show nonspecific findings, particularly if the nidus is not recognized as has been reported in up to 35% of cases due to poor evaluation of cortical bone and thick slices.<sup>20,23</sup> When visible, the nidus is low to intermediate signal on T1 and intermediate to high signal on T2 weighted images. Because of the vascularized stroma, the nidus does often enhance, though reactive surrounding edema may also enhance.<sup>20,21</sup> Internal matrix calcifications are low signal but often too small to be accurately visualized. Reactive bone and soft tissue edema is consistently visualized (Fig. 1) but is not adequate to accurately diagnose this lesion.<sup>23</sup>

Osteblastomas share the same histology as osteoid osteomas, but are a less common tumor. They also typically occur in patients <30 years old and are differentiated from osteoid osteomas by size, where the nidus of an osteblastoma is >2 cm.<sup>20,21,24</sup> Unlike osteoid osteomas, these lesions produce dull pain and soft tissue swelling (not night pain)<sup>20,25</sup> and are more commonly found in the axial skeleton, including the posterior elements of the spine (35-40%) and sacrum (up to 40%), followed by long bone diaphyses (30%).<sup>20,21,26</sup>



CT is also the imaging method of choice because it best characterizes the matrix mineralization, as well as the integrity of the cortex.<sup>20</sup> Generally there is a round or oval radiolucent, well-circumscribed, expansile lesion, measuring >2 cm, with at least partly calcified matrix (Fig. 2). Compared with osteoid osteomas, there tends to be less reactive sclerosis but more periosteal reaction and more aggressive features like bone destruction and soft tissue infiltration.<sup>25-27</sup>

MR imaging features of osteoblastoma are also nonspecific, though are useful to define the extent of osseous involvement and possible extrasosseous soft tissue extension, particularly within the spinal canal.<sup>20,21</sup> Osteoblastomas tend to have a sharply demarcated nidus of low to intermediate signal on T1 and intermediate to high signal on T2 weighted images when nonmineralized, as well as areas of low signal intensity on all sequences when mineralized. These tumors can also demonstrate substantial intraosseous and surrounding soft tissue inflammation (Fig. 2).<sup>20,21</sup>

Osteosarcomas are the second most common primary malignancy of bone, following myeloma.<sup>21,28</sup> They may be primarily osteoblastic (50-80%), chondroblastic (5-25%), or fibroblastic (7-25%),<sup>29,30</sup> and can be divided by differences in cell type, histologic grade, or location in bone into the following: high-grade intramedullary (conventional) osteosarcoma (75%), telangiectatic (4-11%), surface osteosarcomas (4-10%), small cell (1%), intra-osseous low-grade (<1%), maxillofacial or gnathic (1%), and secondary osteosarcoma (5-7%).<sup>21,28,30</sup>

Conventional osteosarcoma is a high-grade intramedullary tumor with peak incidence in the 2<sup>nd</sup> or 3<sup>rd</sup> decades.<sup>28,30</sup> They usually occur in long tubular bones (70-80%), nearly always in the metaphysis (90-95%), particularly about the knee where 35-45% of cases involve the distal femur and 15-20% the proximal tibia.<sup>28,29</sup> Clinically, patients present with pain and swelling and may have limited range of motion of the nearest affected joint. The diagnosis is often suggested by its typical radiographic appearance, including a large mixed lytic and sclerotic lesion with cortical destruction, ill-defined margins, aggressive periosteal reaction (laminated, hair-on-end, Codman triangle, or sunburst patterns), a soft tissue mass, and fluffy or cloud-like osteoid matrix.<sup>12,28,31</sup>

CT is helpful identifying osteoid production which may be subtle and only visible by CT in some tumors.<sup>31</sup> It can also provide a more complete assessment of classic features, including cortical destruction and periosteal reaction (Fig 3). The non-mineralized intraosseous components are more challenging to characterize on CT though replace the normal low attenuation medullary fat with soft tissue density. Areas of necrosis within the tumor are low attenuation but still higher than fat density.<sup>21,28</sup>

MR imaging is the imaging of choice for staging and assessment of the extent of the tumor, including epiphyseal involvement, presence of skip metastases, extraosseous soft tissue invasion, intra-articular spread, and relationship to surrounding structures.<sup>21</sup> These tumors are most commonly low signal on T1 and high signal on T2 weighted images, replacing the normal marrow fat and extending into the adjacent soft tissues through areas of cortical destruction (Fig. 3). Heterogeneous signal is seen in areas of internal hemorrhage and necrosis.<sup>31</sup> Mineralized matrix, dark on all sequences, may be

overlooked or difficult to identify on MR imaging. However, edema and soft tissue characterization are readily seen with fat-suppressed T2 and postcontrast T1 sequences. The extent of peritumoral edema is important and must be reported for appropriate surgical resection, ensuring removal of potential underlying viable tumor cell nests.<sup>21</sup> Contrast enhancement also helps identify viable tumor, which affects both pre- and post-treatment staging.<sup>9</sup>

The next most common osteosarcoma is telangiectatic osteosarcoma. This aggressive variant makes up 4-11% of osteosarcomas and has similar demographic features as conventional osteosarcoma, including mean age, location (most commonly at the knee and generally metaphyseal in long bones), and frequent epiphyseal extension.<sup>28,32,33</sup> Differentiating features include the more common presentation with pathologic fracture (up to 60%) and the characteristic imaging appearance.<sup>21,32</sup>

By definition, telangiectatic osteosarcoma must have hemorrhagic, cystic, or necrotic spaces, lined by malignant cells, that occupy more than 90% of the lesion before treatment.<sup>21,28</sup> The tumor-lined blood-filled cystic spaces demonstrate characteristic fluid-fluid levels (74-90%), as well as aggressive features of osseous expansion, osseous destruction, aggressive periosteal reaction, and matrix mineralization.<sup>28,30,32</sup> The fluid-fluid levels may be confused for benign lesions, namely aneurysmal bone cysts (ABCs), so careful attention to differentiating features, such as peripheral nodularity and extension into the surrounding soft tissues, should be made on CT and MR imaging.

CT is superior at delineating the osseous expansion of the cortex, areas of cortical destruction, pathologic fracture, aggressive periosteal reaction patterns, and matrix mineralization. The latter is an important distinguishing feature from ABCs and is present in up to 58% of cases but nearly always mild, which may be missed on MR imaging in up to 52% of cases.<sup>21,30,32</sup> The cystic spaces demonstrate nonspecific low CT attenuation but heterogeneous fluid signal on MR imaging often with classic fluid-fluid levels from layering hemorrhagic contents. Peripheral nodular soft tissue tumor, also an important distinguishing feature from ABCs, is higher attenuation (similar to muscle) on CT, intermediate to high T1 signal on MR imaging, and enhances after contrast administration on both image techniques.<sup>28,32</sup> Extent of intramedullary disease, presence of cortical destruction with a soft tissue mass (seen in 89% of cases), and identification of joint involvement (44%) and neurovascular encasement (26%) are best seen on MR imaging.<sup>32</sup>

Surface osteosarcomas are another subset of osteosarcoma, making up 4-10% of all osteosarcomas. This group includes intracortical, high grade surface, periosteal, and parosteal osteosarcomas, which vary widely in appearance.

Periosteal osteosarcomas make up 25% of surface osteosarcomas.<sup>28,30</sup> They are highly chondroblastic and frequently non-mineralized, and arise from the deep periosteal surface, typically from a long bone diaphysis, where they tend to produce periosteal reaction perpendicular to the cortex, cortical thickening, and cortical scalloping or saucer-like erosion underlying a broad based surface soft tissue mass that demonstrates high

water content low density on CT and high signal on T2 weighted MR images (Fig. 4).<sup>21,30,34</sup> Unlike parosteal osteosarcomas, intramedullary extension is uncommon and high T2 intramedullary signal on MR imaging represents reactive changes, particularly when not contiguous with the mass.<sup>30,34</sup>

Finally, parosteal osteosarcomas are the commonest of the surface osteosarcomas, comprising 65% of these surface malignancies,<sup>21</sup> and are low-grade tumors growing from the outer layer of the periosteum.<sup>30,35,36</sup> Though commonly cited to occur in skeletally mature patients, a review of more than 200 cases by Okada, et al, demonstrated a mean age of 13 years, ranging from 2-41 years.<sup>36</sup> Despite being low-grade tumors, higher grade features may be seen, including osteoblastic intramedullary invasion in up to 22-50%<sup>35,36</sup> and unmineralized soft tissue at the periphery of the mass in 32% with soft tissue and/or neurovascular invasion in a subset of these cases (Fig. 5).<sup>36</sup> These are best characterized on imaging as an exophytic, cauliflower-like mass with dense central mineralization and a small connecting stalk to the underlying bone, best seen with CT.<sup>9,21</sup> Intraosseous extension, typically osteoblastic (not lytic) is also best identified by CT and may indicate a higher grade tumor.<sup>35</sup> Other signs of higher grade disease include regions of unmineralized soft tissue or a discrete soft tissue mass, particularly when at the periphery of the tumor and if measures more than 1 cm.<sup>3,28,35,36</sup> The presence of a soft tissue mass, while usually visible on CT, is more avidly identified and characterized on MR imaging, where the mass most commonly demonstrates high signal on T2 weighted images.<sup>35</sup>

### *Chondroid Tumors*

Chondroid matrix tumors range from benign tumors, including chondroblastomas, chondromyxoid fibromas, and enchondromas, to malignant tumors, primarily a spectrum of chondrosarcomas.

Chondroblastoma is a rare, benign chondroid tumor (<1% of primary bone tumors) that typically occurs in the epiphysis, or epiphyseal-equivalents, of skeletally immature patients in their 2<sup>nd</sup> decade.<sup>12,37,38</sup> Characteristically located in the epiphyses of long bones (75-80%), these tumors are mostly found in the proximal tibia (25%), distal femur (24%), proximal humerus (23%), and proximal femur (22%), with most others occurring, in the small bones of the feet (talus, calcaneus, and cuboid) or patella.<sup>12,38</sup> Unlike most benign bone lesions, these tumors present with pain in nearly all cases.<sup>38,39</sup>

Radiologically, this tumor presents as a well-defined geographic lytic lesion with lobulated contour eccentrically located in the epiphysis.<sup>12,37,38,40</sup> These tumors may demonstrate a thin sclerotic border and, in up to 30%, scattered matrix mineralization<sup>38,40</sup>, both of which may be radiographically occult and are best seen by CT (Fig. 6). More than half of chondroblastomas demonstrate a nearly pathognomonic pattern of thick, solid periosteal reaction at the metaphysis, distant from the epiphyseal lesion, which is also best seen on CT.<sup>38-41</sup> Active periostitis, on the other hand, may be better seen on MR imaging. In a study by Weatherall and colleagues, only 11 of 22 lesions demonstrated periosteal reaction on CT, but 17 of 22 demonstrated periosteal reaction or edema on MR imaging.

Other important MR imaging features include a well-defined, lobular epiphyseal lesion with intermediate to high signal on T2 weighted images and extensive perilesional bone marrow and soft tissue edema.<sup>38-42</sup> Although there is a classic chondroid lobular contour, the signal on T2 images may not be the water-bright signal seen with most chondroid lesions due to abundant immature matrix and hypercellular chondroblasts (Fig. 6).<sup>38</sup> This appearance, if not recognized, may be mistaken for tumors of other compositions, such as osteblastomas, fibroxanthomas, or giant cell tumors.<sup>40</sup> The perilesional edema (77-100% of cases) is a hallmark of this tumor but can be confused for an inflammatory or infectious processes, such as a Brodie's abscess.<sup>12,39,40</sup> This edema resolves after surgical treatment and can be a helpful sign for tumor recurrence on follow-up imaging.<sup>37</sup>

Chondromyxoid fibroma (CMF) is an even rarer benign chondroid tumor (0.004% of primary bone tumors) typically occurring in young patients (1<sup>st</sup>-3<sup>rd</sup> decades) and may present with pain and swelling.<sup>12,38</sup> Although benign, this tumor may be considered aggressive with high recurrence rate after curettage.<sup>43-45</sup> The tumor is composed of variable quantities of chondroid, myxoid, and fibrous tissues, making the imaging appearance variable and the pathologic diagnosis difficult. Radiologically, CMFs are circumscribed lytic lesions with a narrow zone of transition, sclerotic rim, and scalloped or expanded overlying cortex (Fig. 7). They are typically located eccentrically in the metaphyses of lower extremity long bones (75% of cases), most commonly in the proximal tibia.<sup>12,43-46</sup> CT occasionally demonstrates internal calcified matrix (~15%)<sup>38</sup>. The typical cartilage composition is best seen on MR imaging with intermediate to low

signal on T1 and high signal on T2 weighted images with variable homogeneity based on quantities of chondroid and myxoid tissue in the tumor (Fig. 7).<sup>12,43,45</sup> Periosteal reaction, although rare with these lesions, was also noted by Kim, et al, to have a higher prevalence on MR imaging.<sup>43</sup>

Enchondromas are common benign intramedullary hyaline cartilage tumors (12-24% of benign bone tumors), typically asymptomatic and discovered incidentally in nearly any age group (more often in the 2<sup>nd</sup>-4<sup>th</sup> decades).<sup>9,37,47-50</sup> They are most commonly found in the small bones of the hands (28-60% of cases), followed by the metaphysis or epiphyses of long bones (25%),<sup>38,47-49</sup> and demonstrate the signature appearance of cartilage lesions: a lobular lesion with water density/intensity (due to high water content of cartilage) and variable degrees of internal ring-and-arc mineralized matrix.<sup>9,38,42</sup> When eccentric, endosteal scalloping may also be seen,<sup>9,49,50</sup> but cortical destruction, periosteal reaction, and a soft tissue mass should not be present and suggest a malignant chondroid lesion.

CT is best for confirming “ring-and-arc” matrix mineralization and evaluating endosteal scalloping of enchondromas (Fig. 8). “Ring-and-arc” mineralization is usually present in some quantity (~95%) except for the small bones of the hands and feet where it is rather uncommon.<sup>38,47,49,51</sup> Endosteal scalloping is seen in up to 70-100% of enchondromas depending on the lesion location and is also best seen on CT.<sup>49,50</sup> In a study of 133 cartilage lesions by Santacreu, CT showed twice as many cases (64%) actually involved the cortex compared to only 32% on MR imaging.<sup>52</sup> Murphey and colleagues demonstrated a correlation with malignancy when there is deep endosteal scalloping



(>2/3 the normal cortical thickness).<sup>48</sup> However, if the lesion is eccentric, located in small bones, or an isolated finding, deep scalloping does not necessarily indicate malignancy.<sup>49,50</sup>

MR imaging is the method of choice to demonstrate the signature cartilage appearance of lobular high signal on T2 weighted images (Fig. 8), which is quite specific (79%) but not highly sensitive (35%) for cartilage.<sup>38,42,49,53</sup> The addition of intravenous contrast images with ring-and-arc enhancement increases the sensitivity for cartilage lesions up to 83%.<sup>42</sup>

One of the greatest challenges in assessing enchondromas is distinguishing it from a chondrosarcoma (CS), particularly in long bones.<sup>38,48,50,52,54</sup> Similar to osteosarcomas, there are a number of subtypes of chondrosarcomas, though we will focus on the conventional or central chondrosarcoma as it is by far the most common type.

Chondrosarcomas are the third most common primary bone tumor (8-17% of bone tumors) and usually present in the 5<sup>th</sup> and 6<sup>th</sup> decades, arising de novo (primary) or from a pre-existing lesion such as the cartilage cap of an osteochondroma or from an enchondroma.<sup>37,55,55-57</sup> They usually occur in the metaphyses of long bones (45%), particularly the femur, humerus, and tibia, but they may also be diaphyseal (36%), epiphyseal (16%), or in the axial skeleton where the ilium followed by ribs, scapula, and sternum are more commonly involved.<sup>57</sup> In general, chondrosarcomas are typically large in size (>5 cm) and cause pain, which are important differentiating features from enchondromas (usually <4cm and asymptomatic).<sup>48,52</sup> However, the clinical, imaging,

and pathologic distinction between cellular enchondromas and low grade chondrosarcomas can be extremely difficult.<sup>37,51,54,55</sup>

Low grade chondrosarcomas demonstrate signature cartilage features commonly similar to enchondromas, including ring-and-arc mineralization in up to 60-78% of cases (Fig. 9).<sup>57</sup> However, deep endosteal scalloping (described above), cortical remodeling with permeative or moth-eaten destruction (higher grade CSs), and especially an associated soft tissue mass are distinguishing features of chondrosarcomas (Figs. 9 & 10).<sup>37,48,57</sup> The first two of these characteristics are best delineated on CT, while the latter is best determined with MR imaging. Further, entrapment of the underlying native bone marrow fat is a hallmark feature of low grade CSs differentiating from enchondromas, which is seen as speckled areas of increased T1 signal on MR imaging in up to 35% of cases.<sup>56,57</sup> With higher grade CSs, soft tissue components are more prevalent and areas of trapped bone are less common. Septal and rim enhancement may be seen with low grade CSs on both CT and MR imaging, whereas higher grade lesions may show diffuse enhancement due to greater soft tissue mass component and less well-differentiated cartilage.<sup>42,51,55,57</sup>

### ***Fibrous Tumors***

Fibrous lesions of bone encompass a wide spectrum of benign and malignant tumors or tumor-like conditions. The focus here will be lesions that manifest a recognizable fibrous matrix on imaging.

Fibrous dysplasia is the commonest of these and is a benign lesion of marrow replacement with fibrous tissue containing irregular spindles of largely non-mineralized woven bone.<sup>58,59</sup> It can occur in nearly any bone, present at any age, and is usually monostotic (80%). When polyostotic (20%), it may be seen with various syndromes like McCune Albright and Mazabraud syndromes.<sup>58,60</sup>

Radiologically, fibrous dysplasia is classically a lytic, expansile intramedullary lesion that may demonstrate smooth endosteal scalloping and deformities of long bones, such as the “shepherd’s crook” deformity of the proximal femur or “saber shin” deformity of the tibia.<sup>58-60</sup> CT clearly identifies the typical “ground-glass,” hazy internal appearance of fibrous composition (usually 70-130 Hounsfield units (HU)) with or without a thin sclerotic rim (Fig. 11).<sup>58,59</sup> The degree of ground-glass opacity ranges from nearly completely lytic to diffusely dense and correlates with the histologic degree of fibrous elements (more radiolucent) and woven bone (more radiopaque).<sup>58</sup>

MR imaging is non-specific and the quite variable, typically hypointense on T1 but ranging from hypointense to hyperintense signal on T2 weighted images, depending on the proportions of fibrous tissue, mineralized trabeculae, and cystic or hemorrhagic degeneration (Fig. 11).<sup>60-62</sup> Intravenous contrast enhancement is also variable and potentially confusing as the tissue is relatively vascular with numerous small vessels centrally and large peripheral sinusoids. Thus, they may demonstrate central contrast enhancement (majority) or peripheral enhancement.<sup>62</sup>

Osteofibrous dysplasia (OFD) is a rarer benign fibro-osseous neoplasm (0.2% of primary bone tumors) that typically occurs in the first decade of life and is characteristically found in the tibia (95% of cases).<sup>63-66</sup> Synchronous fibular lesions are seen in up to 12%.<sup>65,66</sup> OFDs are self-limiting and undergo spontaneous regression in puberty<sup>65</sup> but can overlap with the appearance of adamantinomas (AD), a malignant fibrous neoplasm that typically presents in adolescence.

Histologically, OFDs are composed of osteoid, fibrous, and epidermoid tissue.<sup>63,65</sup> Radiologically, these lesions are classically well-defined intracortical expansile lytic lesions, which may be solitary, multilocular, or multifocal, with varying degrees of surrounding sclerosis in the anterior mid tibial diaphyseal cortex (Fig. 12).<sup>66,67</sup> Ground-glass mineralization typical of fibrous lesions is seen in approximately 40% of cases, notably more common than seen in ADs (25% of cases).<sup>67</sup> CT is preferred over MR imaging for characterizing this lesion because it is best at identifying the intracortical location, ground-glass matrix, and intramedullary extension (40% of OFDs). Solid periosteal reaction, tibial bowing, and pathologic fractures are possible findings but not consistently seen.<sup>65,67</sup> MR imaging is less helpful in making the diagnosis but more helpful in planning biopsy approach and surgical staging. There is usually intermediate signal on T1 and heterogeneously intermediate or, less commonly, high signal on T2 weighted images, depending on the cellularity and mineralization (Fig. 12).<sup>66</sup> A thick low intensity rim from the surrounding sclerosis may be seen. Diffuse enhancement is the most common pattern on postcontrast images due to rich fibrovascular stroma similar to other fibro-osseous lesions.<sup>66</sup>

Adamantinoma is a rare low-grade malignant tumor (<0.5% of bone tumors) postulated by some to be in the same disease spectrum as OFD, presenting similarly in location (anterior tibial cortex) and radiologic characteristics.<sup>66-68</sup> Adamantinoma, however, usually presents later (2<sup>nd</sup> or 3<sup>rd</sup> decade in up to 75% of cases) than OFD and with larger lesions (average 13 cm vs 6 cm) and more aggressive features than OFD on imaging, such as skip lesions (38%), “moth-eaten” (up to 88%) or destroyed cortex (38%), complete medullary involvement (67-88%), and extraosseous soft tissue extension (15%) (Fig. 13).<sup>65-67</sup>

Other fibrous tumors of bone include benign entities such as desmoplastic fibromas and benign fibrous histiocytomas, as well as malignant lesions such as fibrosarcomas and malignant fibrous histiocytomas (MFH). These tumors represent a range of non-aggressive lytic to very aggressive destructive lesions of bone and have less specific imaging appearances, thus are only briefly mentioned here. In general, fibrosarcomas and malignant fibrous histiocytoma (MFH) are indistinguishable by imaging and demonstrate geographic, moth-eaten, or permeative cortical destruction, commonly in long bones.<sup>69,70</sup> CT is best for evaluating cortical destruction, and MR imaging is useful in determining intraosseous extent and soft tissue involvement.

### ***Vascular bone tumors***

Vascular lesions of bone also range in their histologic grade, of which the most commonly encountered lesion is the hemangioma. Hemangiomas are benign, slow-

growing vascular neoplasms composed of a mixture of vessels, fat, smooth muscle, fibrous tissue, and clotted blood.<sup>71,72</sup> They are most commonly found in women in the 4<sup>th</sup>-5<sup>th</sup> decades, primarily in the spine. The classic CT appearance of spine lesions is diagnostic and includes a well-circumscribed hypodense lesion with a “corduroy” (coronal or sagittal plane) or “polka dot” (axial plane) appearance due to coarsened trabecula. The MR appearance of vertebral hemangiomas is dependent on the quantity of fatty stroma versus vascular elements, the former of which is more prevalent in classic lesions and produces hyperintensity on T1 that fat-suppresses. These lesions are hyperintense on T2 weighted images regardless of composition due to the vascular elements.

The much rarer appendicular hemangioma is extremely varied in appearance. Generally, these lesions are well-defined, lobular lytic intramedullary lesions, though some appear aggressive with moth-eaten margins, an associated soft tissue component, and/or perilesional bone marrow and soft tissue edema.<sup>71,72</sup> They may demonstrate coarsened trabeculae, a key to the imaging diagnosis, or internal mineralization, both of which are best seen on CT.<sup>71,72</sup> Cortical thinning or erosion is seen on CT in 29% and 7% of cases, respectively.<sup>71</sup> The MR appearance is strikingly different from vertebral lesions with iso- to hypointense signal on T1 images. Hyperintensity on T2 and variable heterogeneous enhancement is typical but nonspecific. The low signal intensity trabecular pattern is seen in only 42% on MR imaging and is better characterized with CT.<sup>71</sup> Ultimately, because of their varied appearance, pathologic diagnosis is required.<sup>72</sup>

Malignant vascular tumors (MVT) of bone are also quite rare (<1% of primary malignant bones tumors) and demonstrate a varied and nonspecific appearance. This category of lesions includes low-grade hemangioendotheliomas and their epithelioid variants to high grade angiosarcomas. They are more commonly found in lower extremity long bones and are always osteolytic, variably expansile, and often heterogeneous in density/signal with avid but heterogeneous enhancement, varying somewhat depending on grade of the tumor.<sup>73</sup> An associated soft tissue mass and cortical destruction are common, but there is characteristically no periosteal reaction.<sup>73,74</sup> CT best depicts the presence and degree of cortical destruction and reactive cortical sclerosis, whereas soft tissue extension and reactive change may be better identified on MR. MR features include ill-defined high signal on T2-weighted images and enhancement, extending into the surrounding bone and soft tissues, mostly due to reactive edema based on pathologic correlation.<sup>73</sup>

### ***Fat origin tumors***

Several of the tumors described to this point have had components of fat, including areas of trapped marrow fat in low-grade chondrosarcomas and fatty stroma of hemangiomas. However, bone tumors with fat composition or origin are another category of tumors for consideration when differentiating primary bone tumors on imaging.

Intraosseous lipomas are the most common fat-containing primary bone tumor (<0.1% of all bone tumors). Although cited as very rare, the prevalence may be much greater by anecdotal reports from Murphey and colleagues due to its incidental nature. These tumors are located in long bones, most commonly the femur (34%), and other characteristic

locations such as the calcaneus (8%) and ilium near the sacroiliac joint (8%).<sup>75</sup> The radiographic appearance is nonspecific, but CT and MR are usually diagnostic with fat clearly visible by both techniques.<sup>75,76</sup> CT demonstrates a circumscribed hypodense lesion, measuring -60 to -100 HU, with a thin calcified rim (Fig. 14)<sup>75</sup>. MR imaging similarly demonstrates high signal on T1 and T2 weighted images, similar to subcutaneous fat, with signal loss on fat-suppressed sequences.<sup>75,76</sup> Gradient echo imaging, where calcification displays bold hypointense signal, may also be helpful to delineate the calcified rim and a central calcified “scar”.<sup>76</sup> Adjacent normal marrow fat has a slightly higher density on CT and slightly lower T1 signal on MR imaging due to cellular marrow elements.<sup>75</sup> Evolution of these lesions, classified by Milgram and colleagues, results in signal changes, most notably central areas of ring-like or dystrophic “central scar” calcification with lesion maturation and fat necrosis.<sup>77</sup> This appearance is essentially diagnostic of an intraosseous lipoma on CT and MR imaging. At times, these lesions may be confused with osteonecrosis or chondroid lesions, but the generally rounded margins helps distinguish the lesion as a lipoma rather than either differential entity.<sup>75,78</sup>

Another tumor to consider when analyzing a fat-containing lesion is a liposarcoma of bone, a primary bone malignancy arising from lipoblasts that follows a similar course as soft tissue liposarcomas. These tumors are extremely rare with less than 100 reported in the literature. CT and MR imaging reveals predominantly fat-containing lesions but demonstrate aggressive features, including cortical erosion/destruction and an extraosseous extension of a soft tissue mass.<sup>79</sup>



### ***Round cell tumors***

The final group of tumors we will discuss includes a mix of tumors with common cellular and imaging features rather than cell origin or tissue composition. These tumors (collectively round cell tumors) include myeloma, lymphoma, and Ewing sarcoma, and share the common histology of being highly cellular tumors composed of homogeneous undifferentiated, basophilic, cytoplasm-poor, round cells.<sup>12</sup>

Myeloma, although arguably a marrow tumor, is considered the most common primary malignancy of bone,(27% of biopsied bone tumors).<sup>12,37</sup> It can occur anywhere but classically affects the skull and axial skeleton, followed by the appendicular skeleton. Patients typically present at >40 years with either local symptoms of pain/pathologic fractures or systemic marrow symptoms.<sup>37</sup>

The variable imaging appearance results from cellular activation of osteoclasts and inhibition of osteoblasts by myeloma cells, resulting in bone destruction.<sup>9,12</sup> There may be a solitary or multiple focal well-defined lytic lesions with a “punched out” appearance and nonsclerotic narrow or wide zone of transition (Fig. 15). Although skeletal survey is still recommended as the gold standard for initial screening and staging, PET-CT and whole body MRI are more sensitive and increase the yield for detection of myeloma lesions.<sup>80-82</sup>

CT will reveal a focal lytic lesion without internal matrix, and internal soft tissue density helps differentiate from other lytic etiologies, such as a bone cyst or fibrous dysplasia. More sensitive than CT or radiographs, MR imaging demonstrates one of the following four patterns: normal bone marrow, a micronodular (salt-and-pepper) appearance, a focal lesion, or diffuse marrow abnormality.<sup>80,83</sup> A typical myeloma lesion demonstrates hypointense T1 signal, homogeneous hyperintense T2 signal, and diffuse contrast enhancement (Fig. 15).<sup>9,12,37</sup> These lesions are typically round, central intramedullary lesions, though endosteal or full thickness cortical erosion may be seen. Cortical breakthrough and soft tissue extension are not uncommon and are particularly well characterized by MR imaging.<sup>37</sup> Diffuse disease, also detected best by MR imaging, may demonstrate diffuse heterogeneous signal with innumerable areas of the signal described above.

Primary lymphoma of bone is another small round cell tumor in the differential diagnosis of myeloma, and is defined as lymphoma affecting one or multiple bones, generally without lymph node involvement. This form of lymphoma is uncommon (3-5% of malignant bone tumors and 4-5% of extranodal lymphomas)<sup>9,12,84</sup> and typically present in the 4<sup>th</sup>-6<sup>th</sup> decade with a painful soft tissue mass or systemic symptoms.<sup>12,37,84</sup> These tumors are most commonly found in the metadiaphysis of long bones (71%) like the femur, humerus, and tibia, followed by flat bones (22%) such as the pelvis and skull.<sup>84,85</sup>

Characteristic imaging features of primary bone lymphoma include involvement of a large portion of the affected bone, a soft tissue mass extending through an intact cortex,

and a permeative or moth-eaten appearance if macroscopic cortical involvement is present (Fig. 16).<sup>9,12,84</sup> Periosteal reaction has been variably reported from none to just over half of cases<sup>9,85</sup>. A diffusely sclerotic variant is seen in only 2% of primary bone lymphomas, such as with the classic “ivory vertebra” appearance of an entirely sclerotic vertebral body<sup>37</sup>. CT provides greater detail of cortical involvement, including better depiction of cortical integrity despite extraosseous tumor spread and moth-eaten or permeative destruction when present,<sup>9,12,37</sup> and may also identify bony sequestra,(11-16% of cases).<sup>12,85</sup> MR imaging is highly dependable for identifying intramedullary replacement, tumor extent, and extraosseous soft tissue involvement, which may be present without radiographic signs of cortical destruction (up to 80%) or detection of a soft tissue mass (up to 63% of radiographs and 20% of CTs)<sup>85</sup>. This pattern is also seen with other small round cell tumors, such as Ewing sarcoma. A distinguishing feature of lymphoma’s soft tissue mass is the propensity to insinuate into adjacent soft tissues and cross compartments without displacing or compressing structures like the neurovascular bundle (Fig. 16).<sup>12</sup> The marrow signal characteristics are variable due to the degree of fibrous tissue and cellularity, but are generally low on T1 and intermediate to high on T2 weighted sequences.<sup>85</sup> The use of fat-suppression is important as these lesions may be similar to marrow fat on non-fat suppressed T2 images.<sup>12</sup>

Ewing sarcoma is the third most common primary bone sarcoma (~12% of malignant bone tumors) and is a small round cell tumor but originates from primitive neuroectodermal tissue.<sup>12,37</sup> These tumors, which occur in a young population (usually <20 years old), are highly malignant and most often occur in the pelvis (31%) or long

bone diaphysis (62% of peripheral skeleton). Occasional metaphyseal involvement is noted with very rare epiphyseal extension.<sup>12,86</sup> These aggressive tumors produce a painful mass and may produce systemic symptoms that overlap with infection.<sup>12,37</sup>

The characteristic radiologic imaging appearance is that of a lytic, destructive lesion with wide zone of transition, aggressive periosteal reaction (classically onion-skin or lamellated), and a large soft tissue mass.<sup>12,30,37</sup> Although these lesions are most commonly mixed lytic and sclerotic (75%), there is no true matrix production, consistent with its small round cell composition.<sup>12,86</sup> Uncommonly, there may be cortical thickening and reactive sclerosis from tumor response or saucerization of the cortex due to periosteal surface destruction by tumor cells and soft tissue mass-related extrinsic pressure.<sup>12</sup> The periosteal reaction and pattern of bone destruction, including tumor margin classification, is best identified by CT. Frouge, et al, found that spiculated periosteal reaction and Codman's triangle were the most common patterns,<sup>87</sup> though Resnick and Kransdorf cite lamellated reaction as most common (57%).<sup>88</sup> When aggressive, the pattern of periosteal reaction may be confused for osteosarcoma in the pelvis or axial skeleton. Increased density from the intramedullary component may be underestimated on CT<sup>12,86</sup>. Thus, MR imaging is best to define the intramedullary extent and tumor margins as well as extraosseous soft tissue mass, which is often more expansive than the intramedullary component (Fig. 17).<sup>37,86,87</sup> Because this aggressive tumor often has a large soft tissue component, it is of highest importance to clearly characterize involvement of surrounding soft tissues, including neurovascular bundles and multicompartiment spread. Although the above described features are helpful in making the diagnosis, the MR signal

characteristics are not specific to the tumor, typically demonstrating inhomogeneous intermediate to low signal on T1 and high signal on T2 with hypocellular regions and areas of necrosis demonstrating lower signal on T1 and higher signal on T2.<sup>12,37</sup>

Postcontrast sequences may help delineate tumor and differentiate from surrounding peritumoral edema.

## CONCLUSION

Identifying the tumor matrix or composition, which is often more sensitive by CT and MR imaging as has been discussed, is helpful to accurately characterize a tumor. These cross sectional imaging techniques also delineate secondary features to help characterize lesion aggressiveness and extent. Ultimately, radiographs should always be performed and may make the diagnosis of a bone tumor, but CT and MR imaging are useful adjunct methods to help differentiate lesions when necessary, stage tumors, and guide management, including biopsy planning and execution.

## REFERENCES

1. Dorfman HD, Czerniak B, Kotz R, Vanel D, Park YK, Unni KK. WHO Classification of Bone Tumours.
2. Franchi A. Epidemiology and classification of bone tumors. *Clin Cases Miner Bone Metab.* 2012;9(2):92-95.
3. Unni KK, Inwards CY, Bridge JA, Kindblom LG, Wold LE. *Tumors of the Bones and Joints: AFIP Atlas of Tumor Pathology.* Silver Spring, MD: American Registry of Pathology; 2005.
4. Balach T, Stacy GS, Peabody TD. The clinical evaluation of bone tumors. *Radiol Clin North Am.* 2011;49(6):1079-1093, v. doi:10.1016/j.rcl.2011.07.001.

5. Enneking WF. A system of staging musculoskeletal neoplasms. *Clin Orthop*. 1986;(204):9-24.
6. Sherman C, O'Connor M. Musculoskeletal Tumor Imaging: An Orthopedic Oncologist Perspective. *Semin Musculoskelet Radiol*. 2013;17(02):221-226. doi:10.1055/s-0033-1343098.
7. Morrison W, Weissman B, Kransdorf M, et al. ACR Appropriateness Criteria: Primary Bone Tumors. *Am Coll Radiol*. 2013. <https://acsearch.acr.org/docs/69421/Narrative/>. Accessed November 23, 2016.
8. Nomikos G, Murphey M, Kransdorf M, Bancroft L, Peterson J. Primary bone tumors of the lower extremities. *Radiol Clin North Am*. 2002;40(5):971-990.
9. Teo HEL, Peh WCG. Primary bone tumors of adulthood. *Cancer Imaging*. 2004;4(2):74-83. doi:10.1102/1470-7330.2004.0004.
10. Hapani H, Kalola J, Hapani J. Comparative role of CT scan and MR imaging in primary malignant bone tumors. *IOSR J Dent Med Sci*. 2014;13(11):29-35.
11. Parsons T, Frink S, Campbell S. Musculoskeletal Neoplasia: Helping the Orthopaedic Surgeon Establish the Diagnosis. *Semin Musculoskelet Radiol*. 2007;11(1):003-015. doi:10.1055/s-2007-984411.
12. Greenspan A, Jundt G, Remagen W. *Differential Diagnosis in Orthopaedic Oncology*. 2nd ed. Philadelphia, PA: Lippincott Williams & Wilkins; 2007.
13. Hogeboom WR, Hoekstra HJ, Mooyaart EL, et al. MRI or CT in the preoperative diagnosis of bone tumours. *Eur J Surg Oncol J Eur Soc Surg Oncol Br Assoc Surg Oncol*. 1992;18(1):67-72.
14. Zimmer WD, Berquist TH, McLeod RA, et al. Bone Tumors: Magnetic Resonance Imaging versus Computed Tomography. *Radiology*. 1985;155:709-718.
15. Stacy GS, Mahal RS, Peabody TD. Staging of bone tumors: a review with illustrative examples. *AJR Am J Roentgenol*. 2006;186(4):967-976. doi:10.2214/AJR.05.0654.
16. Kransdorf M, Bridges M. Current Developments and Recent Advances in Musculoskeletal Tumor Imaging. *Semin Musculoskelet Radiol*. 2013;17(02):145-155. doi:10.1055/s-0033-1343070.
17. Disler DG, McCauley TR, Ratner LM, Kesack CD, Cooper JA. In-phase and out-of-phase MR imaging of bone marrow: prediction of neoplasia based on the detection of coexistent fat and water. *Am J Roentgenol*. 1997;169(5):1439-1447. doi:10.2214/ajr.169.5.9353477.

18. Wakabayashi H, Saito J, Taki J, et al. Triple-phase contrast-enhanced MRI for the prediction of preoperative chemotherapeutic effect in patients with osteosarcoma: comparison with <sup>99m</sup>Tc-MIBI scintigraphy. *Skeletal Radiol.* 2016;45(1):87-95. doi:10.1007/s00256-015-2250-1.
19. Miller T. Bone Tumors and Tumorlike Conditions: Analysis with Conventional Radiography. *Radiology.* 2008;246(3):662-674.
20. Cerase A, Priolo F. Skeletal benign bone-forming lesions. *Eur J Radiol.* 1998;27, Supplement 1:S91-S97. doi:10.1016/S0720-048X(98)00049-7.
21. White LM, Kandel R. Osteoid-Producing Tumors of Bone. *Semin Musculoskeletal Radiol.* 2000;4(01):0025-0044. doi:10.1055/s-2000-6853.
22. Klein MH, Shankman S. Osteoid osteoma: radiologic and pathologic correlation. *Skeletal Radiol.* 1992;21(1):23-31. doi:10.1007/BF00243089.
23. Davies M, Cassar-Pullicino VN, Davies AM, McCall IW, Tyrrell PNM. The diagnostic accuracy of MR imaging in osteoid osteoma. *Skeletal Radiol.* 2002;31(10):559-569. doi:10.1007/s00256-002-0546-4.
24. McLeod R, Dahlin D, Beabout J. The spectrum of osteoblastoma. *Am J Roentgenol.* 1976;126(2):321-325. doi:10.2214/ajr.126.2.321.
25. Yalcinkaya U, Doganavsargil B, Sezak M, et al. Clinical and morphological characteristics of osteoid osteoma and osteoblastoma: a retrospective single-center analysis of 204 patients. *Ann Diagn Pathol.* 2014;18(6):319-325. doi:10.1016/j.anndiagpath.2014.08.006.
26. Arockiaraj J, Balaji G G, Vidyasagar B, Ashok A. Osteoblastoma of the coracoid process: an unusual location. *BMJ Case Rep.* 2015;2015. doi:10.1136/bcr-2015-212070.
27. Della Rocca C, Huvos AG. Osteoblastoma: varied histological presentations with a benign clinical course. An analysis of 55 cases. *Am J Surg Pathol.* 1996;20(7):841-850.
28. Murphey MD, Robbin MR, McRae GA, Flemming DJ, Temple HT, Kransdorf MJ. The many faces of osteosarcoma. *RadioGraphics.* 1997;17(5):1205-1231. doi:10.1148/radiographics.17.5.9308111.
29. Dahlin DC, Coventry MB. Osteogenic Sarcoma. *J Bone Jt Surg Am.* 1967;49(1):101-110.
30. Rajiah P, Ilaslan H, Sundaram M. Imaging of Primary Malignant Bone Tumors (Nonhematological). *Radiol Clin North Am.* 2011;49(6):1135-1161. doi:10.1016/j.rcl.2011.07.003.

31. Park SK, Lee IS, Cho KH, Lee YH, Yi JH, Choi KU. Osteosarcoma of pelvic bones: imaging features. *Clin Imaging*. 2017;41:59-64. doi:10.1016/j.clinimag.2016.10.013.
32. Murphey MD, wan Jaovisidha S, Temple HT, Gannon FH, Jelinek JS, Malawer MM. Telangiectatic osteosarcoma: radiologic-pathologic comparison. *Radiology*. 2003;229(2):545-553. doi:10.1148/radiol.2292021130.
33. Huvos AG, Rosen G, Bretsky SS, Butler A. Telangiectatic osteogenic sarcoma: a clinicopathologic study of 124 patients. *Cancer*. 1982;49(8):1679-1689.
34. Murphey MD, Jelinek JS, Temple HT, Flemming DJ, Gannon FH. Imaging of periosteal osteosarcoma: radiologic-pathologic comparison. *Radiology*. 2004;233(1):129-138. doi:10.1148/radiol.2331030326.
35. Jelinek JS, Murphey MD, Kransdorf MJ, Shmookler BM, Malawer MM, Hur RC. Parosteal osteosarcoma: value of MR imaging and CT in the prediction of histologic grade. *Radiology*. 1996;201(3):837-842. doi:10.1148/radiology.201.3.8939240.
36. Okada K, Frassica FJ, Sim FH, Beabout JW, Bond JR, Unni KK. Parosteal osteosarcoma. A clinicopathological study. *J Bone Jt Surg Am*. 1994;76(3):366-378.
37. Lewis VO, Morris CD, Parsons TW. Malignant and benign bone tumors that you are likely to see. *Instr Course Lect*. 2013;62:535-549.
38. Douis H, Saifuddin A. The imaging of cartilaginous bone tumours. I. Benign lesions. *Skeletal Radiol*. 2012;41:1195-1212.
39. Yamamura S, Sato K, Sugiura H, Iwata H. Inflammatory reaction in chondroblastoma. *Skeletal Radiol*. 1996;25(4):371-376. doi:10.1007/s002560050097.
40. Weatherall PT, Maale GE, Mendelsohn DB, Sherry CS, Erdman WE, Pascoe HR. Chondroblastoma: classic and confusing appearance at MR imaging. *Radiology*. 1994;190(2):467-474. doi:10.1148/radiology.190.2.8284401.
41. Brower AC, Moser RP, Kransdorf MJ. The frequency and diagnostic significance of periostitis in chondroblastoma. *Am J Roentgenol*. 1990;154(2):309-314. doi:10.2214/ajr.154.2.2105021.
42. De Beuckeleer LHL, De Schepper AMA, Ramon F, Somville J. Magnetic resonance imaging of cartilaginous tumors: a retrospective study of 79 patients. *Eur J Radiol*. 1995;21(1):34-40. doi:10.1016/0720-048X(96)81067-9.
43. Kim H-S, Jee W-H, Ryu K-N, et al. MRI of chondromyxoid fibroma. *Acta Radiol*. 2011;52(8):875-880. doi:10.1258/ar.2011.110180.



44. Lersundi A, Mankin HJ, Mourikis A, Hornicek FJ. Chondromyxoid fibroma: a rarely encountered and puzzling tumor. *Clin Orthop*. 2005;439:171-175.
45. Durr HR, Lienemann A, Nerlich A, Stumpfenhausen B, Refior HJ. Chondromyxoid fibroma of bone. *Arch Orthop Trauma Surg*. 2000;120:42-47.
46. Budny AM, Ismail A, Osher L. Chondromyxoid fibroma. *J Foot Ankle Surg Off Publ Am Coll Foot Ankle Surg*. 2008;47(2):153-159. doi:10.1053/j.jfas.2007.08.013.
47. Hong ED, Carrino JA, Weber KL, Fayad LM. Prevalence of shoulder enchondromas on routine MR imaging. *Clin Imaging*. 2011;35(5):378-384. doi:10.1016/j.clinimag.2010.10.012.
48. Walden MJ, Murphey MD, Vidal JA. Incidental enchondromas of the knee. *AJR Am J Roentgenol*. 2008;190(6):1611-1615. doi:10.2214/AJR.07.2796.
49. Bierry G, Kerr DA, Nielsen GP, et al. Enchondromas in children: imaging appearance with pathological correlation. *Skeletal Radiol*. 2012;41(10):1223-1229. doi:10.1007/s00256-012-1377-6.
50. Bui KL, Ilaslan H, Bauer TW, Lietman SA, Joyce MJ, Sundaram M. Cortical scalloping and cortical penetration by small eccentric chondroid lesions in the long tubular bones: not a sign of malignancy? *Skeletal Radiol*. 2009;38(8):791-796. doi:10.1007/s00256-009-0675-0.
51. Vanel D, Kreshak J, Larousserie F, et al. Enchondroma vs. chondrosarcoma: A simple, easy-to-use, new magnetic resonance sign. *Eur J Radiol*. 2013;82(12):2154-2160. doi:10.1016/j.ejrad.2011.11.043.
52. Ferrer-Santacreu EM, Ortiz-Cruz EJ, Díaz-Almirón M, Pozo Kreilinger JJ. Enchondroma versus Chondrosarcoma in Long Bones of Appendicular Skeleton: Clinical and Radiological Criteria-A Follow-Up. *J Oncol*. 2016;2016:8262079. doi:10.1155/2016/8262079.
53. Sampath Kumar V, Tyrrell PNM, Singh J, Gregory J, Cribb GL, Cool P. Surveillance of intramedullary cartilage tumours in long bones. *Bone Jt J*. 2016;98-B(11):1542-1547. doi:10.1302/0301-620X.98B11.37864.
54. Wang XL, De Beuckeleer LH, De Schepper AM, Van Marck E. Low-grade chondrosarcoma vs enchondroma: challenges in diagnosis and management. *Eur Radiol*. 2001;11(6):1054-1057. doi:10.1007/s003300000651.
55. Masciocchi C, Sparvoli L, Barile A. Diagnostic imaging of malignant cartilage tumors. *Eur J Radiol*. 1998;27:S86-S90.
56. Yoo HJ, Hong SH, Choi J-Y, et al. Differentiating high-grade from low-grade chondrosarcoma with MR imaging. *Eur Radiol*. 2009;19(12):3008-3014. doi:10.1007/s00330-009-1493-4.

57. Douis H, Saifuddin A. The imaging of cartilaginous bone tumours. II. Chondrosarcoma. *Skeletal Radiol.* 2013;42(5):611-626. doi:10.1007/s00256-012-1521-3.
58. Fitzpatrick KA, Taljanovic MS, Speer DP, et al. Imaging findings of fibrous dysplasia with histopathologic and intraoperative correlation. *AJR Am J Roentgenol.* 2004;182(6):1389-1398. doi:10.2214/ajr.182.6.1821389.
59. Daffner R, Kirks D, Gehweiler J, Heaston D. Computed tomography of fibrous dysplasia. *Am J Roentgenol.* 1982;139(5):943-948. doi:10.2214/ajr.139.5.943.
60. Rubin AN, Byrns K, Zhou D, Freedman L. Fibrous Dysplasia of the Rib: AIRP Best Cases in Radiologic-Pathologic Correlation. *Radiogr Rev Publ Radiol Soc N Am Inc.* 2015;35(7):2049-2052. doi:10.1148/rg.2015140335.
61. Bloem JL, Reidsma II. Bone and soft tissue tumors of hip and pelvis. *Eur J Radiol.* 2012;81(12):3793-3801. doi:10.1016/j.ejrad.2011.03.101.
62. Jee WH, Choi KH, Choe BY, Park JM, Shinn KS. Fibrous dysplasia: MR imaging characteristics with radiopathologic correlation. *Am J Roentgenol.* 1996;167(6):1523-1527. doi:10.2214/ajr.167.6.8956590.
63. Simoni P, Scarciolla L, Mutijima E, Zobel BB. Osteofibrous dysplasia: A case report and review of the literature. *Radiol Case Rep.* 2011;6(4):Article 546. doi:10.2484/rcr.v6i4.546.
64. Lee RS, Weitzel S, Eastwood DM, et al. Osteofibrous dysplasia of the tibia. *Bone Jt J.* 2006;88-B(5):658-664. doi:10.1302/0301-620X.88B5.17358.
65. Bethapudi S, Ritchie DA, MacDuff E, Straiton J. Imaging in osteofibrous dysplasia, osteofibrous dysplasia-like adamantinoma, and classic adamantinoma. *Clin Radiol.* 2014;69(2):200-208. doi:10.1016/j.crad.2013.09.011.
66. Jung J-Y, Jee W-H, Hong SH, et al. MR Findings of the Osteofibrous Dysplasia. *Korean J Radiol.* 2014;15(1):114. doi:10.3348/kjr.2014.15.1.114.
67. Khanna M, Delaney D, Tirabosco R, Saifuddin A. Osteofibrous dysplasia, osteofibrous dysplasia-like adamantinoma and adamantinoma: correlation of radiological imaging features with surgical histology and assessment of the use of radiology in contributing to needle biopsy diagnosis. *Skeletal Radiol.* 2008;37(12):1077. doi:10.1007/s00256-008-0553-1.
68. Ramanoudjame M, Guinebretière J-M, Mascard E, Seringe R, Dimeglio A, Wicart P. Is there a link between osteofibrous dysplasia and adamantinoma? *Orthop Traumatol Surg Res.* 2011;97(8):877-880. doi:10.1016/j.otsr.2011.09.008.
69. Murphey MD, Gross TM, Rosenthal HG. From the archives of the AFIP. Musculoskeletal malignant fibrous histiocytoma: radiologic-pathologic correlation.

*Radiogr Rev Publ Radiol Soc N Am Inc.* 1994;14(4):807-826; quiz 827-828.  
doi:10.1148/radiographics.14.4.7938770.

70. Taconis WK, Mulder JD. Fibrosarcoma and malignant fibrous histiocytoma of long bones: Radiographic features and grading. *Skeletal Radiol.* 1984;11(4):237-245.  
doi:10.1007/BF00351347.
71. Rigopoulou A, Saifuddin A. Intraosseous hemangioma of the appendicular skeleton: imaging features of 15 cases, and a review of the literature. *Skeletal Radiol.* 2012;41(12):1525-1536.  
doi:http://dx.doi.org.proxy.ulib.uits.iu.edu/10.1007/s00256-012-1444-z.
72. Chawla A, Singrakhia M, Maheshwari M, Modi N, Parmar H. Intraosseous haemangioma of the proximal femur: imaging findings. *Br J Radiol.* 2006;79(944):e64-e66. doi:10.1259/bjr/53131368.
73. Xu J-X, Yang L, Chen Y, et al. Differential CT and MR imaging diagnosis between low- and high-grade malignant vascular tumors of bone. *SpringerPlus.* 2016;5(1).  
doi:10.1186/s40064-016-3471-z.
74. Vermaat M, Vanel D, Kroon HM, et al. Vascular tumors of bone: Imaging findings. *Eur J Radiol.* 2011;77(1):13-18. doi:10.1016/j.ejrad.2010.06.052.
75. Murphey MD, Carroll JF, Flemming DJ, Pope TL, Gannon FH, Kransdorf MJ. From the archives of the AFIP: benign musculoskeletal lipomatous lesions. *Radiogr Rev Publ Radiol Soc N Am Inc.* 2004;24(5):1433-1466. doi:10.1148/rg.245045120.
76. Öztekin Ö, Argin M, Oktay A, Arkun R. Intraosseous lipoma: radiological findings. *Radiol Bras.* 2008;41(2):81-86. doi:10.1590/S0100-39842008000200005.
77. Milgram JW. Intraosseous lipomas: radiologic and pathologic manifestations. *Radiology.* 1988;167(1):155-160. doi:10.1148/radiology.167.1.3347718.
78. Mannem RR, Mautz AP, Baynes KE, Zambrano EV, King DM. AIRP best cases in radiologic-pathologic correlation: intraosseous lipoma. *Radiogr Rev Publ Radiol Soc N Am Inc.* 2012;32(5):1523-1528. doi:10.1148/rg.325115031.
79. Macmull S, Atkinson HDE, Saso S, Tirabosco R, O'Donnell P, Skinner JA. Primary intra-osseous liposarcoma of the femur: a case report. *J Orthop Surg.* 2009;17(3):374-378.
80. Hanrahan CJ, Christensen CR, Crim JR. Current Concepts in the Evaluation of Multiple Myeloma with MR Imaging and FDG PET/CT. *RadioGraphics.* 2010;30(1):127-142. doi:10.1148/rg.301095066.
81. Dimopoulos M, Terpos E, Comenzo RL, et al. International myeloma working group consensus statement and guidelines regarding the current role of imaging

techniques in the diagnosis and monitoring of multiple Myeloma. *Leukemia*. 2009;23(9):1545-1556.

82. Mahnken AH, Wildberger JE, Gehbauer G, et al. Multidetector CT of the spine in multiple myeloma: comparison with MR imaging and radiography. *AJR Am J Roentgenol*. 2002;178(6):1429-1436. doi:10.2214/ajr.178.6.1781429.
83. Mouloupoulos LA, Varma DG, Dimopoulos MA, et al. Multiple myeloma: spinal MR imaging in patients with untreated newly diagnosed disease. *Radiology*. 1992;185(3):833-840. doi:10.1148/radiology.185.3.1438772.
84. Singh T, Satheesh CT, Lakshmaiah KC, et al. Primary bone lymphoma: a report of two cases and review of the literature. *J Cancer Res Ther*. 2010;6(3):296-298. doi:10.4103/0973-1482.73366.
85. Mulligan ME, McRae GA, Murphey MD. Imaging features of primary lymphoma of bone. *AJR Am J Roentgenol*. 1999;173(6):1691-1697. doi:10.2214/ajr.173.6.10584821.
86. Peersman B, Vanhoenacker FM, Heyman S, et al. Ewing's sarcoma: imaging features. *JBR-BTR Organe Soc R Belge Radiol SRBR Orgaan Van K Belg Ver Voor Radiol KBVR*. 2007;90(5):368-376.
87. Frouge C, Vanel D, Coffre C, Couanet D, Contesso G, Sarrazin D. The role of magnetic resonance imaging in the evaluation of Ewing sarcoma. *Skeletal Radiol*. 1988;17(6):387-392. doi:10.1007/BF00361656.
88. Davies AM, Sundaram M, James SJ. *Imaging of Bone Tumors and Tumor-Like Lesions: Techniques and Applications*. Springer Science & Business Media; 2009.

**FIGURE CAPTIONS**

Fig. 1. Osteoid osteoma of the humerus in an 8-year-old boy. (A) Axial CT image demonstrates an ovoid radiolucent cortically-based nidus (white arrow) with foci of central mineralization and moderate surrounding sclerosis and cortical thickening (white arrowheads). (B) Sagittal fat-suppressed T2 (T2FS) MR image exhibits the demarcated hyperintense osteoid nidus (white arrow) with extensive surrounding bone marrow edema. Note the normal marrow fat signal intensity in the humeral head epiphysis (asterisk). (C) Axial gradient echo MR image depicts the hypointense mineralization within the osteoid nidus (white arrow) and cortical thickening (white arrowheads).

Fig. 2. Osteoblastoma of the spine (left T11 pedicle and transverse process) in a 14-year-old girl who presented with new-onset painful scoliosis. (A) Axial CT image demonstrates a relatively large, well-demarcated, mildly expansile lucent lesion of the posterior elements of T11 with a thick sclerotic rim and mild surrounding sclerosis (black arrowheads). Axial T1 precontrast (B) and T1 postcontrast (C) MR images demonstrate a hypointense, diffusely enhancing lesion in the left T11 pedicle and transverse process (white arrowheads) with surrounding reactive inflammation (black arrows, (C)).

Fig. 3. Conventional osteosarcoma of the distal femur in an 8-year-old boy. (A) Sagittal CT image demonstrates an aggressive osteosclerotic lesion of the distal femur with destruction of the anterior cortex, a Codman triangle of aggressive periosteal reaction (white arrow), and a soft tissue mass that is non-mineralized posteriorly (open arrowheads) and partly mineralized anteriorly (white arrowheads). (B) Sagittal modified inversion recovery (MODIR) MR image demonstrates the extraosseous soft tissue mass extending through the anterior and posterior cortex (open arrowheads) and surrounding peritumoral edema (white arrows). (C) Coronal T1 MR image demonstrates the extent of the intramedullary hypointense mass replacing the normal marrow fat (white arrows) and periosteal reaction (white arrow heads).

Fig. 4. Periosteal osteosarcoma of the mid femur discovered in a 33-year-old man. (A) AP radiograph demonstrates a thick and irregular proximal lateral right femoral diaphysis

with a mineralized mass extending outward from the surface of the bone cranially (white arrow) and saucerization of the cortex caudally (arrowheads). Coronal fat-suppressed T1 (T1FS) postcontrast (B) and axial T2 (C) MR images demonstrate the hypointense signal of tumor mineralization (white arrow), as well as the solid, enhancing soft tissue mass arising from the surface of the lateral proximal femur (open arrowheads) and intraosseous reactive edema (black asterisk). T1 images (not shown here) demonstrated no abnormal marrow replacement.

Fig. 5. High-grade parosteal osteosarcoma of the distal femur in a 31-year-old male. (A) Lateral radiograph reveals a large centrally ossified mass arising from the posterior distal femoral metadiaphysis (black asterisk) with a thin lucent cleft between the mass and cortex (black dashed arrows), a distinguishing feature of parosteal osteosarcomas. Scattered peripheral mineralization (white arrowheads) reveals the large size of the soft tissue mass, indicating a higher grade tumor. (B) Sagittal T1 MR image shows a large T1 hypointense mass centered posterior to the distal femoral metadiaphysis with central hypointense ossified matrix and intramedullary extension (white asterisk). (C) Axial T1FS post-contrast MR image delineates the mass and soft tissue involvement, including sciatic nerve (black arrow) and femoral artery (white arrow) displacement and encasement (confirmed by operative report), as well as intramedullary extension (white asterisk).

Fig. 6. Chondroblastoma of the proximal tibial epiphysis in a 13-year-old boy. (A) Coronal CT image depicts a well-defined round lytic lesion within the proximal tibial epiphysis with scattered internal “ring-and-arc” chondroid matrix mineralization (white arrow). (B) Coronal STIR MR image demonstrates a heterogeneous intermediate-to-high T2 signal lesion (differing from typical high signal of cartilage due to dense immature cells), a thin hypointense sclerotic rim (white arrowheads), extensive surrounding bone marrow edema (asterisks), and periosteal edema distally along the medial proximal tibial metadiaphysis (white arrows).

Fig. 7. Chondromyxoid fibroma of the posterior iliac wing in a 29-year-old man. (A) Axial CT image shows a well-defined lytic lesion (white arrowheads) with slightly lobular contours, a sclerotic rim, and low attenuation of 30-40 HU. (B) Axial T2FS MR image again demonstrates the lobular lesion (white arrowheads) with hyperintense signal, a thin hypointense low signal rim, and no adjacent edema or extraosseous mass. This lesion diffusely enhanced on postcontrast images (not shown here), confirming a solid lesion.

Fig. 8. Enchondroma of the distal femur in a 59-year-old man. (A) Coronal CT image of the distal femur shows a circumscribed lytic lesion with thin peripherally calcified rim (white arrowhead) and internal “ring-and-arc” calcified chondroid matrix (white arrow). (B) Coronal STIR MR image displays a markedly hyperintense lesion with lobular contours (open arrowheads) and scattered internal hypointense foci (white arrow) of mineralized matrix, both of which are features characteristic of a chondroid lesion.

Fig. 9. Low-grade chondrosarcoma of the proximal tibia in a 30-year-old woman. (A) Sagittal CT image demonstrates a mildly expansile lytic lesion with lobular contours, dense central “ring-and-arc” mineralization, and endosteal scalloping with scattered areas of cortical breakthrough (dashed arrows). (B) Sagittal STIR MR image also demonstrates the posterior proximal tibial epiphyseal/metaphyseal lesion with hyperintense signal, lobular contours (white arrowheads), central hypointense mineralization, and areas of cortical breakthrough with soft tissue mass extension (dashed arrows).

Fig. 10. High-grade chondrosarcoma of the distal femur in an 83-year-old woman. (A) Lateral radiograph reveals an irregular poorly circumscribed lytic lesion of the distal femoral metadiaphysis with anterior cortical destruction (white arrowheads) and “ring-and-arc” matrix mineralization (white arrow). (B) Sagittal T1 MR image also shows a large isointense intramedullary mass with central hypointense mineralization (white arrow) and extraosseous soft tissue extension into the prefemoral fat pad through a large cortical defect (white arrowheads).

Fig. 11. Fibrous dysplasia of the humeral diaphysis in a 9-year-old girl. (A) Sagittal CT image of the humerus exhibits a circumscribed, eccentric, slightly expansile intramedullary lytic lesion (white arrow) with internal ground-glass opacity measuring approximately 120 HU. Sagittal T1 (B) and T1FS post-contrast (C) MR images acquired 7 years later demonstrate the same ovoid, eccentric, intramedullary lesion (white arrow) in the humeral diaphysis with isointense signal (to muscle) on T1 images and diffuse contrast enhancement on post-contrast images.

Fig. 12. Osteofibrous dysplasia of the anterior tibial cortex in a 10-year-old girl. (A) Sagittal CT image exhibits an intracortical multilocular lytic lesion of the anterior proximal tibial diaphysis with surrounding sclerosis and thickened but intact cortex (white arrowheads). Sagittal STIR (B) and axial T1 (C) MR images show hyperintense and intermediate signal intensity, respectively, of the intracortical lytic lesions with intact overlying cortex (white arrowheads), sclerotic margins, and cortical thickening (open arrowheads). The axial image also depicts the partial width intramedullary extension with adjacent normal marrow fat (black asterisk).

Fig. 13. Adamantinoma of the anterior tibial cortex in a 20-year-old man. (A) Lateral radiograph of the tibia and fibula shows a multilocular cortically-based lytic lesion with anterior cortical expansion (white arrows) and diffuse medullary extension. Sagittal STIR (B) and axial T1 (C) MR images demonstrate a somewhat aggressive lesion compared to the OFD of Fig. 12 with areas of anterior tibial cortical destruction and soft tissue extension (white arrows). Involvement of the entire axial medullary space (low signal in (C)), a feature more characteristic of adamantinoma than OFD, is recognized when compared to normal fibular marrow fat (black arrow).

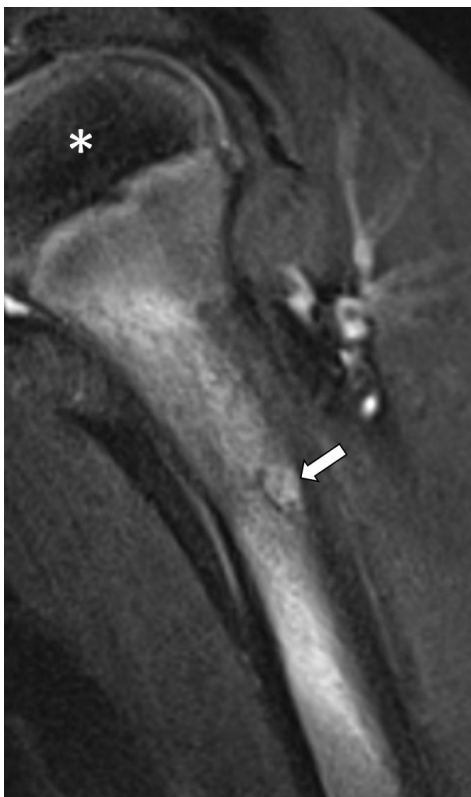
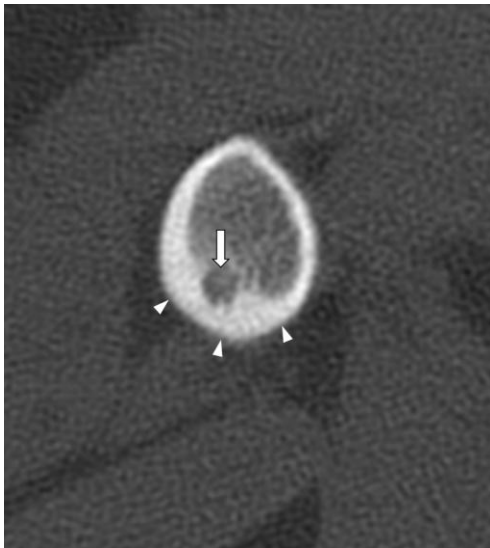
Fig. 14. Intraosseous lipoma of the calcaneus in a 49-year-old man. Sagittal CT image of the ankle demonstrates a circumscribed lucent lesion with sclerotic margins and internal density equal to the subcutaneous fat or Kager's fat pad (white star), consistent with an intraosseous lipoma.



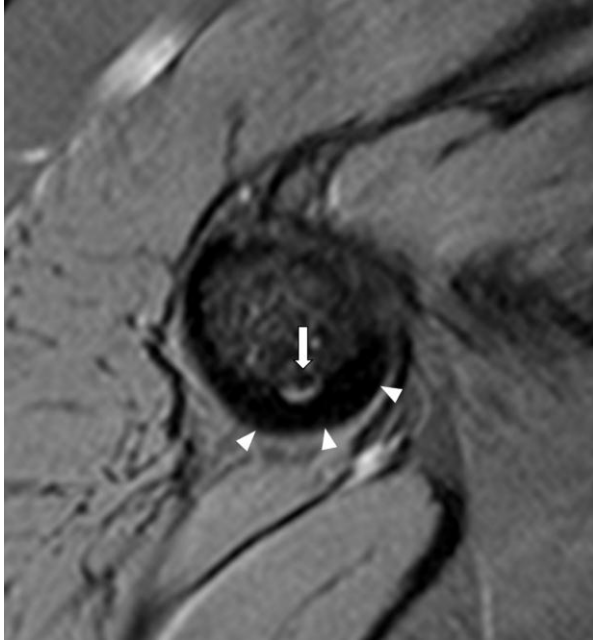
Fig. 15. Multiple myeloma of the distal clavicle in a 68-year-old man. (A) Frontal radiograph of the shoulder reveals a well-defined, “punched out” lytic lesion of the distal clavicle (white arrowheads) with a superimposed pathologic fracture (black arrow). Incidentally, calcific tendinosis (dashed white arrow) is also seen. (B) Coronal STIR MR image shows a mildly hyperintense solid lesion of the distal clavicle with complete marrow replacement and bony expansion (white arrowheads). Additional radiographically-occult myelomatous lesions are discovered in the proximal humeral metadiaphysis (white arrow), which demonstrates high signal compared to the normal marrow fat of the humeral head.

Fig. 16. Primary bone lymphoma of the proximal tibia in a 35-year-old woman. (A) Axial contrast enhanced CT image demonstrates ill-defined low attenuation (white arrows) in the muscles and soft tissues surrounding the tibial diaphysis. (B) Axial T2FS MR image shows the diffuse marrow signal abnormality (asterisk) of the proximal tibial diaphysis with intact cortex and a large surrounding soft tissue mass (white arrows) that involves all of the muscle compartments of the calf, extends into the pretibial subcutaneous tissues, and encases the posterior tibial artery (white arrowhead) without displacement or compression. (C) Coronal T1 MR image delineates the extent of low signal marrow replacement spanning nearly the entire proximal two thirds of the tibia.

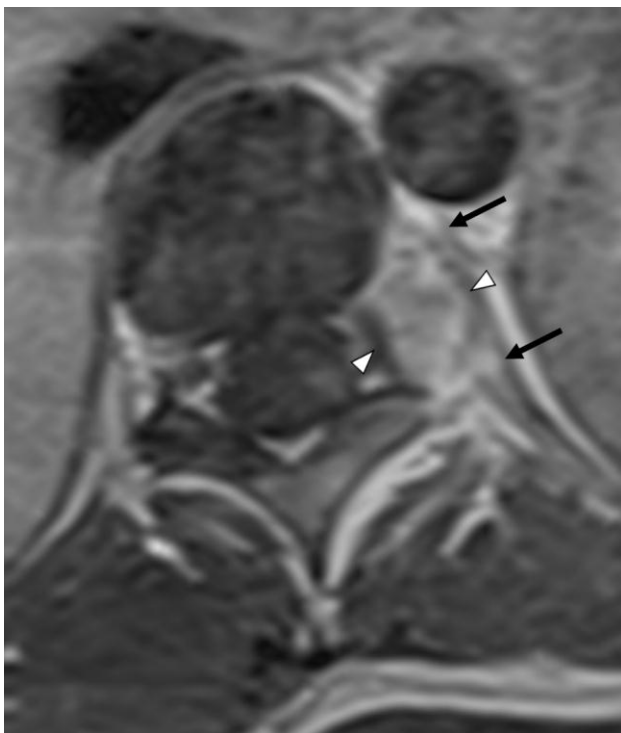
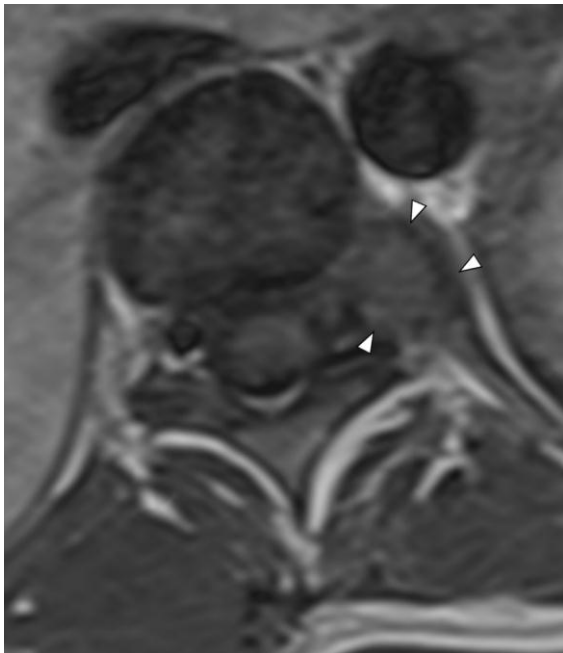
Fig. 17. Ewing sarcoma of the fibula in a 17-year-old girl. (A) Axial contrast enhanced CT image of the proximal calf shows an ill-defined low attenuation mass (white arrows) involving the anterior and deep posterior compartments of the proximal calf. (B) Axial STIR MR image more clearly depicts a hyperintense soft tissue mass (white arrows) centered around the proximal fibula, involving multiple muscle compartments, as well as diffuse bone marrow signal abnormality of the proximal fibula (dashed arrow).



Accepted Manuscript



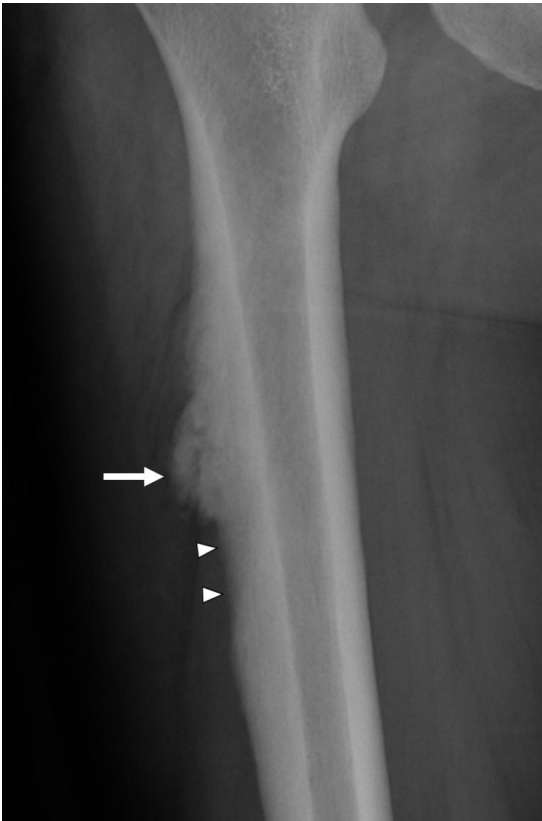
Manuscript



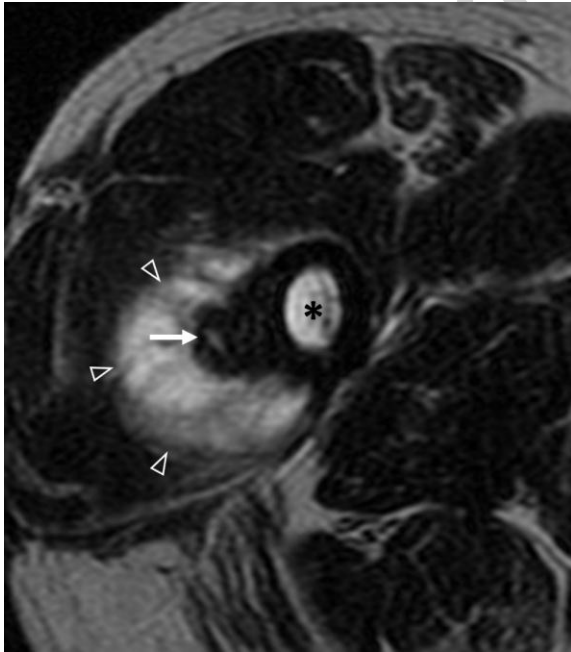
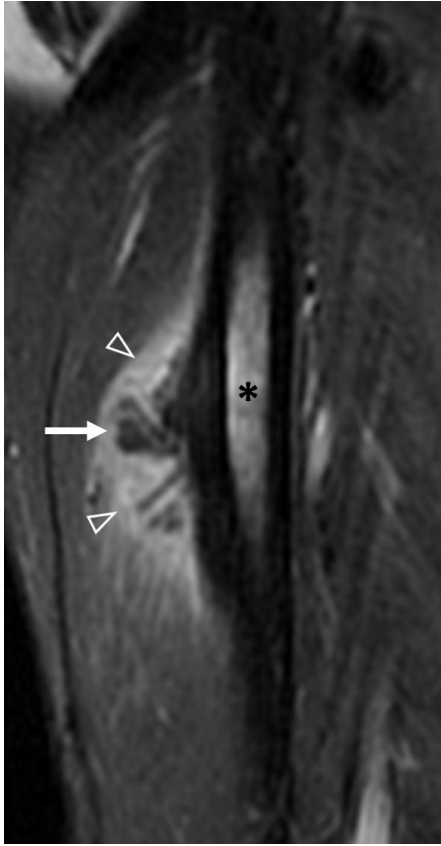
Manuscript

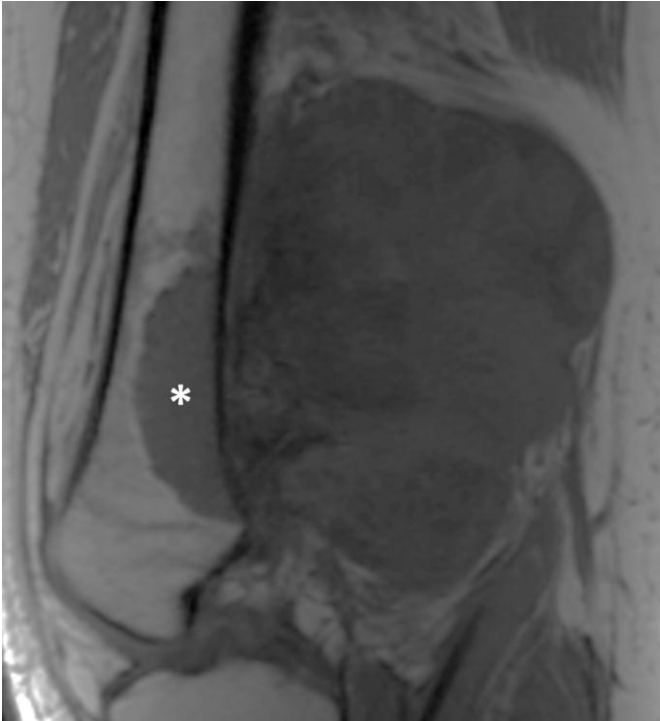
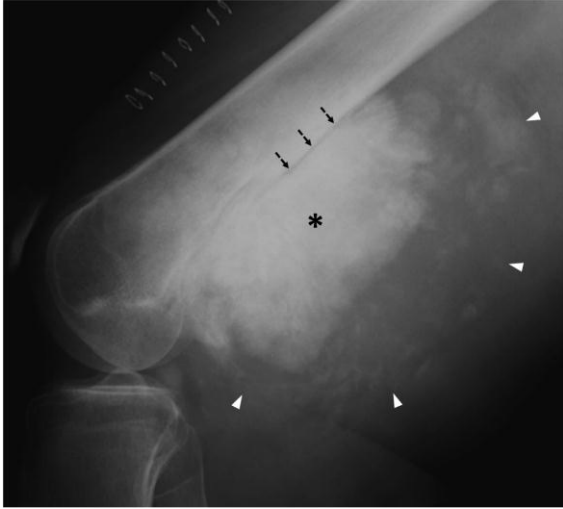


manuscript



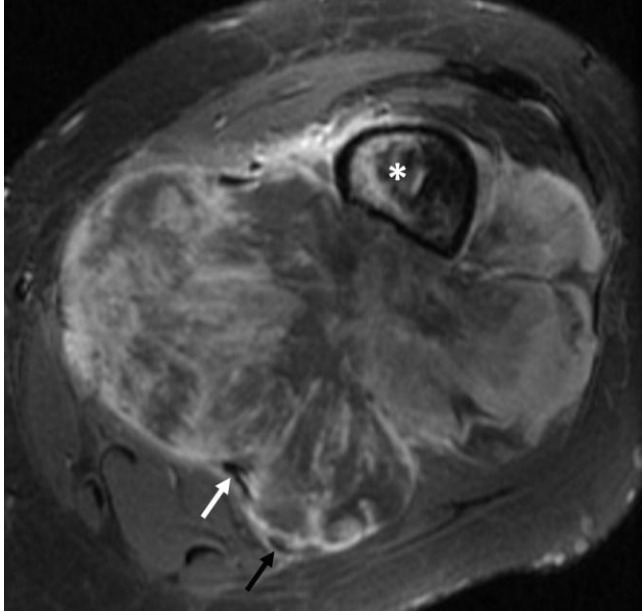
manuscript



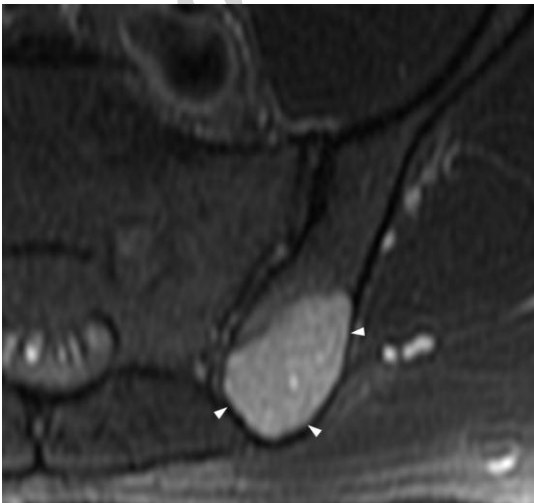
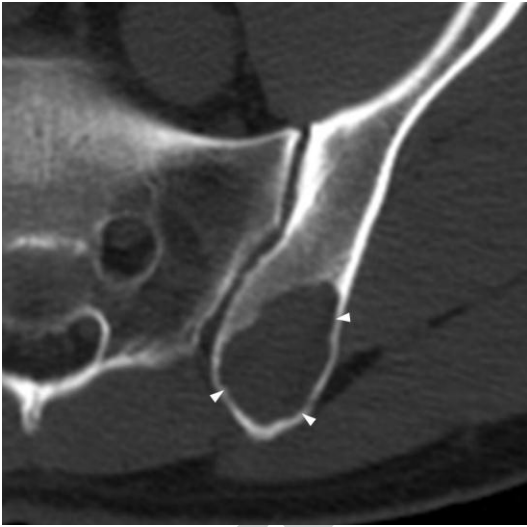


Manuscript

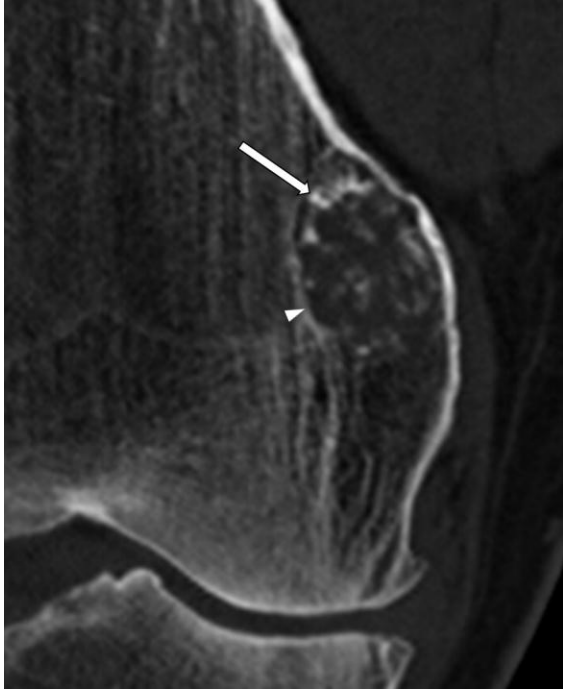




manuscript

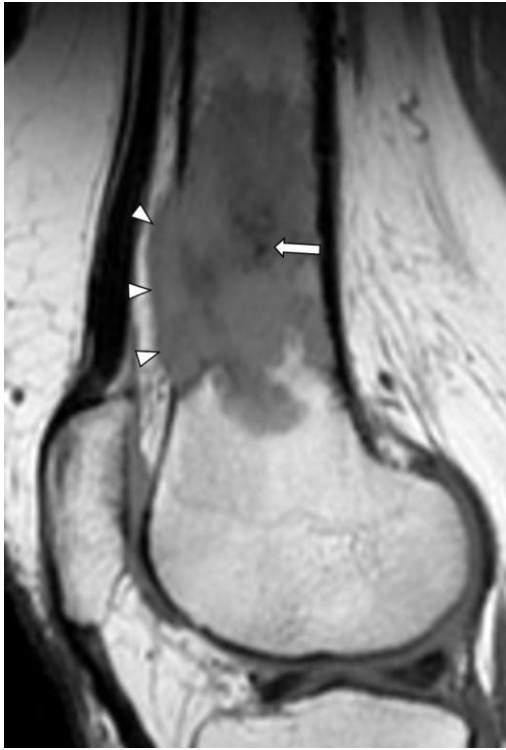


manuscript

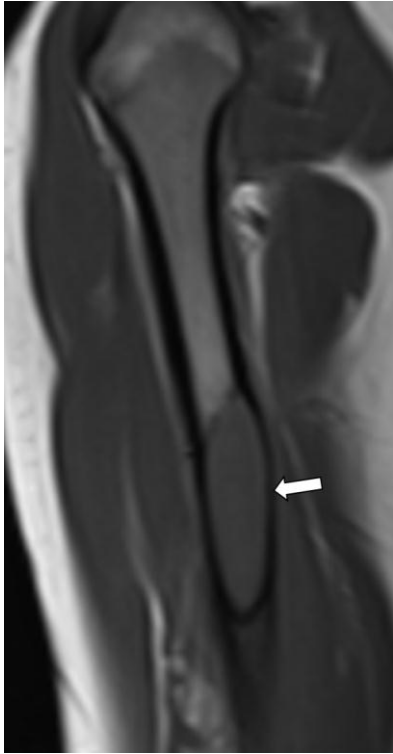


manuscript





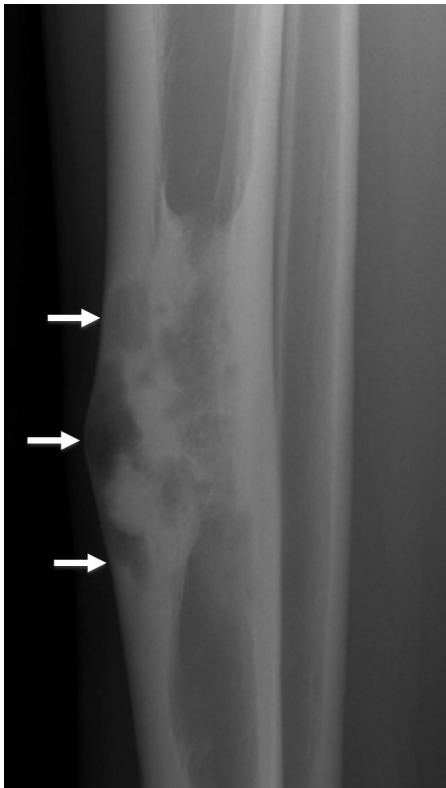
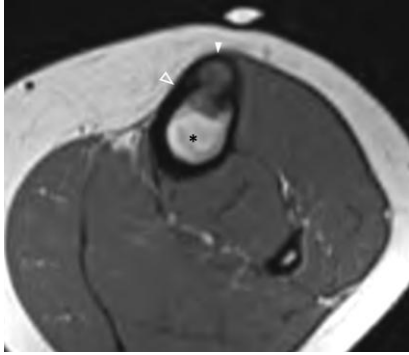
ed manuscript



Accepted manuscript

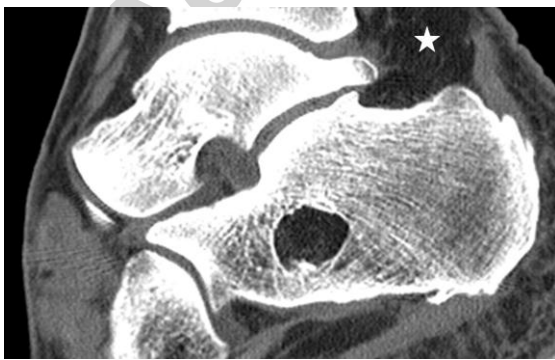
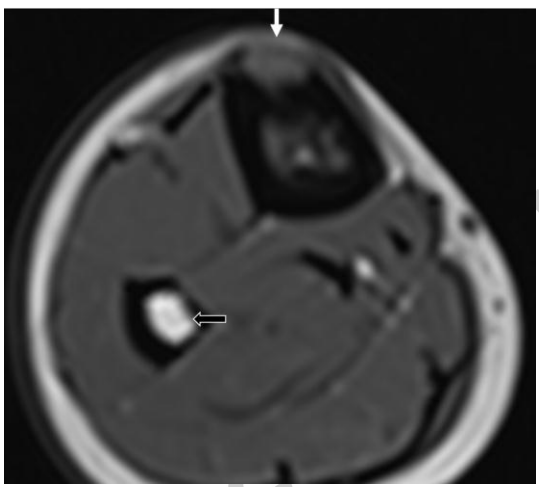
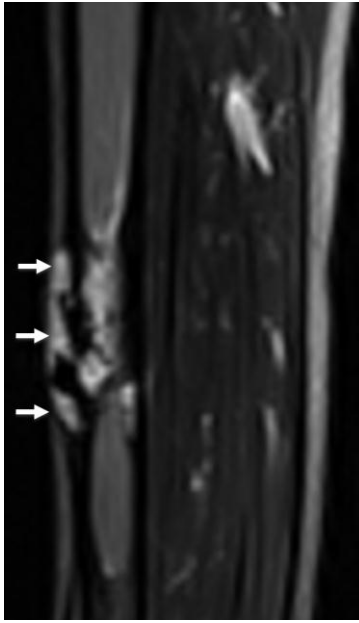


Accepted manuscript

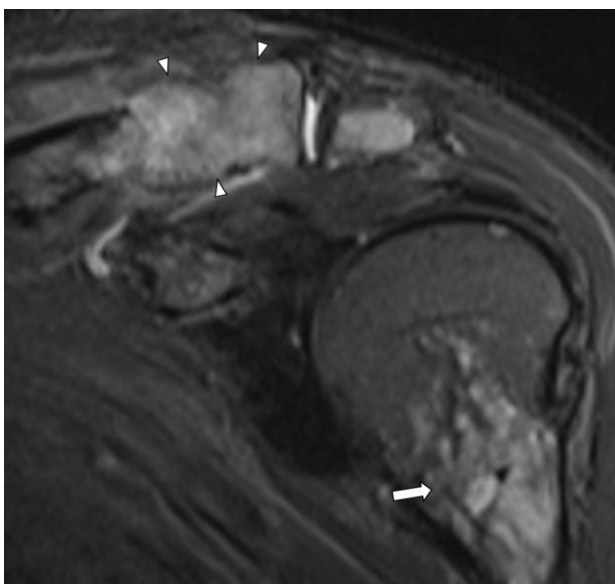
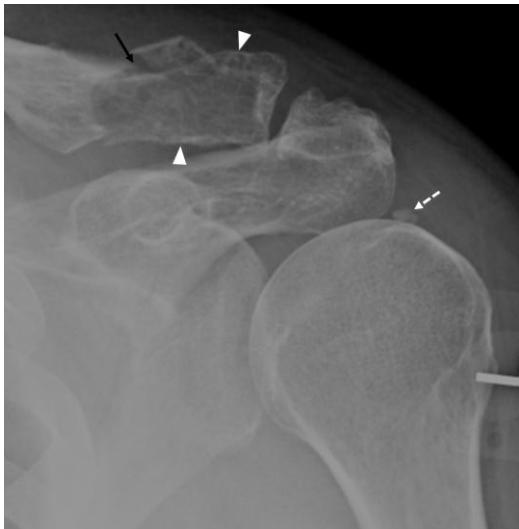


Accepted manuscript



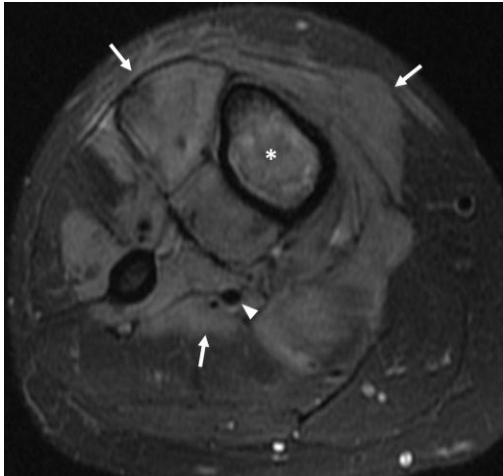


manuscript

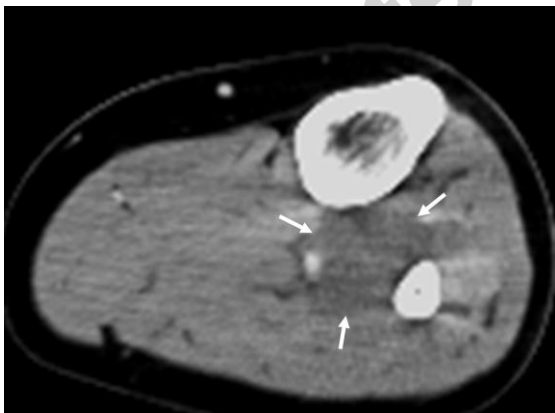
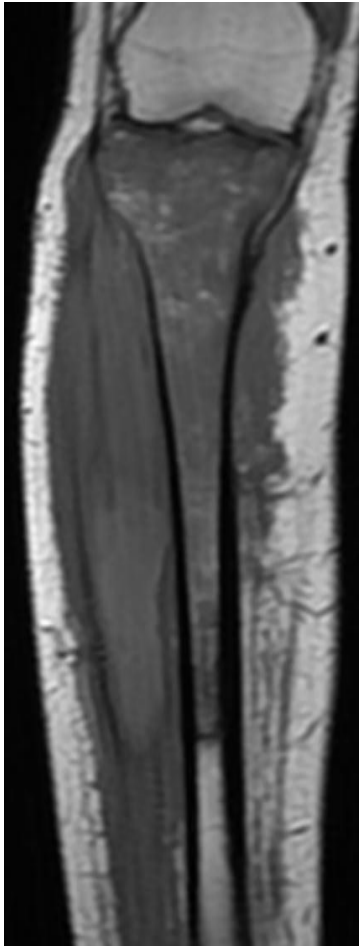


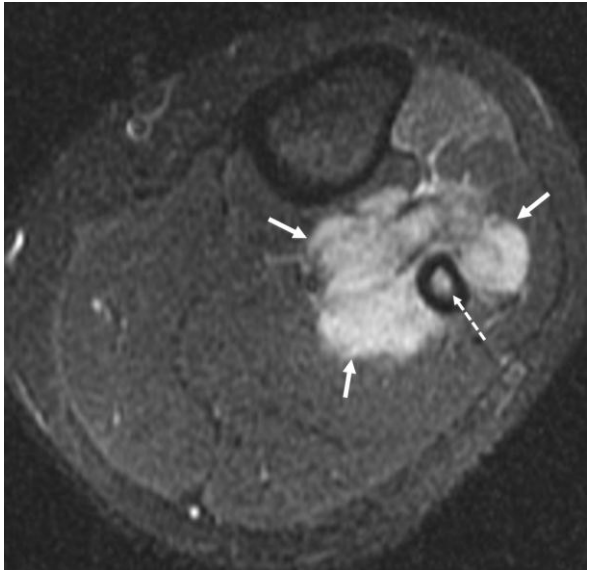
manuscript

ACCEPTED



Accepted manuscript





Accepted manuscript